Cancer Research

miR-450a Acts as a Tumor Suppressor in Ovarian Cancer by Regulating Energy Metabolism

Bruna Rodrigues Muys[1,2,3,4,5], Josane F. Sousa[1,2,3,6], Jessica Rodrigues Plaça[1,2,3], Luíza Ferreira de Araújo[1,2,3,7], Aishe A. Sarshad[4], Dimitrios G. Anastasakis[4], Xiantao Wang[4], Xiao Ling Li[5], Greice Andreotti de Molfetta[1,2,3], Anelisa Ramão[1,2], Ashish Lal[5], Daniel Onofre Vidal[8], Markus Hafner[4], and Wilson A. Silva[1,2,3]

Abstract

Dysregulation of miRNA expression is associated with multiple diseases, including cancers, in which small RNAs can have either oncogenic or tumor suppressive functions. Here we investigated the potential tumor suppressive function of miR-450a, one of the most significantly downregulated miRNAs in ovarian cancer. RNA-seq analysis of the ovarian cancer cell line A2780 revealed that overexpression of miR-450a suppressed multiple genes involved in the epithelial-to-mesenchymal transition (EMT). Overexpression of miR-450a reduced tumor migration and invasion and increased anoikis in A2780 and SKOV-3 cell lines and reduced tumor growth in an ovarian tumor xenographic model. Combined AGO-PAR-CLIP and RNA-seq analysis identified a panel of potential miR-450a targets, of which many, including TIMMDC1, MT-ND2, ACO2, and ATP5B, regulate energetic metabolism. Following glutamine withdrawal, miR-450a overexpression decreased mitochondrial membrane potential but increased glucose uptake and viability, characteristics of less invasive ovarian cancer cell lines. In summary, we propose that miR-450a acts as a tumor suppressor in ovarian cancer cells by modulating targets associated with glutaminolysis, which leads to decreased production of lipids, amino acids, and nucleic acids, as well as inhibition of signaling pathways associated with EMT.

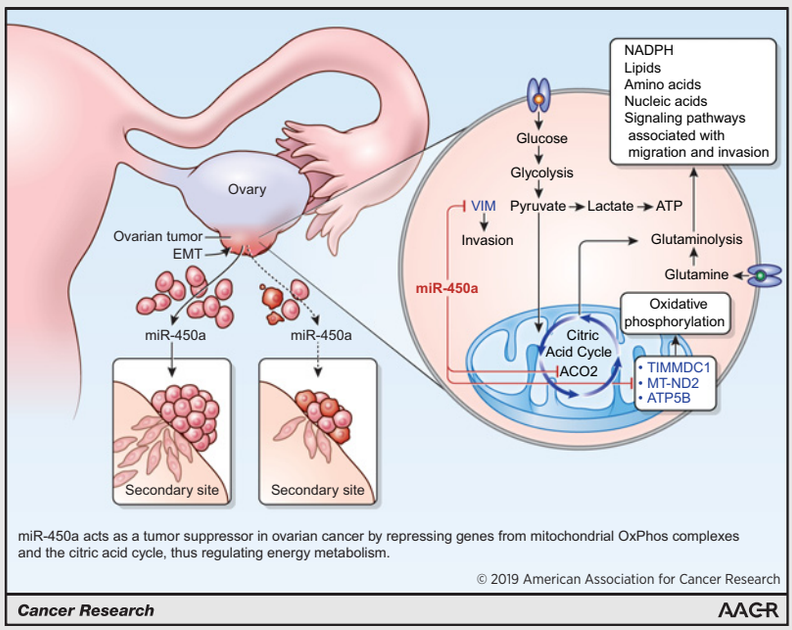

miR-450a acts as a tumor suppressor in ovarian cancer by repressing genes from mitochondrial OxPhos complexes and the citric acid cycle, thus regulating energy metabolism.

Significance: miR-450a limits the metastatic potential of ovarian cancer cells by targeting a set of mitochondrial mRNAs to reduce glycolysis and glutaminolysis.

Graphical Abstract: http://cancerres.aacrjournals.org/content/canres/79/13/3294/F1.large.jpg.

[1]Department of Genetics, Ribeirão Preto Medical School, University of São Paulo, Ribeirão Preto, Brazil. [2]Center for Cell-Based Therapy (CEPID/FAPESP), National Institute of Science and Technology in Stem Cell and Cell Therapy (INCTC/CNPq), Regional Blood Center of Ribeirão Preto, Ribeirão Preto, Brazil. [3]Center for Medical Genomics (HCFMRP/USP), Center for Integrative Systems Biology (CISBi–NAP/USP), Ribeirão Preto, Brazil. [4]Laboratory of Muscle Stem Cells and Gene Regulation, National Institute for Arthritis and Musculoskeletal and Skin Disease, Bethesda, Maryland. [5]Regulatory RNAs and Cancer Section, Genetics Branch, Center for Cancer Research, NCI, NIH, Bethesda, Maryland. [6]Genetics and Molecular Biology Program, Institute of Biological Sciences, Federal University of Para-UFPA, Belem, Brazil. [7]Medical Genomics Laboratory, AC Camargo Cancer Center, São Paulo, Brazil. [8]Molecular Oncology Research Center, Barretos Cancer Hospital, Barretos, Brazil.

Note: Supplementary data for this article are available at Cancer Research Online (http://cancerres.aacrjournals.org/).

Corresponding Authors: Markus Hafner, NIH, 50 South Drive, Rm 1154, Bethesda, MD 20892. Phone: 240-676-5791; Fax: 301-480-9699; E-mail: markus.hafner@nih.gov; and Wilson A. Silva, Department of Genetics, Ribeirão Preto Medical School, University of São Paulo, Avenida Bandeirantes 3900, Monte Alegre, Ribeirão Preto, SP, CEP: 14049-900, Brazil. Phone: 5516-2101-9362; E-mail: wilsonjr@usp.br

Cancer Res 2019;79:3294–305

doi: 10.1158/0008-5472.CAN-19-0490

Introduction

Ovarian cancer is the most lethal gynecologic tumor worldwide, largely due to a lack of specific symptoms and reliable biomarkers (1). As a consequence, 75% of patients are already in an advanced stage at the time of diagnosis and only 30% can be cured (2). Therefore, there is an urgent need to develop biomarkers capable to help diagnose ovarian cancer earlier, as well as to identify targets to improve treatment.

miRNAs, noncoding RNAs of 21–23 nucleotides length, play a key role in posttranscriptional regulation of gene expression of most mRNAs (3). Together with Argonaute (AGO) proteins miRNAs form the core of the RNA-induced silencing complex (RISC) silencing target RNAs. miRNAs guides RISC to its targets, mainly by limited base-pairing by 6–8 nucleotides at the 5′ end of the miRNA, the so called seed sequence (4, 5). On the target RNA, AGO recruits a number of accessory proteins including the TNRC6A-C scaffolding protein and the CCR4-NOT deadenylase complex, resulting in mRNA deadenylation, which in turn triggers mRNA decapping and destabilization and translational repression (6–8). Most miRNAs recognize multiple target mRNAs, so that each of the 90 most conserved miRNA families target more than 400 different mRNAs, resulting in most mammalian mRNAs being predicted to be regulated by miRNAs (9). Knockout studies confirmed that many of these conserved miRNAs are required for normal development and physiology (3). Consistently, dysregulation of miRNA levels has been associated with tumorigenesis and many miRNAs have been characterized as oncogenes or tumor suppressors (10).

There is abundant evidence of miRNA dysregulation in ovarian cancer (11). For instance, in samples from late-stage epithelial ovarian cancer more than 40 miRNAs, among them miR-450a, were found downregulated compared with early-stage disease (12). Similarly, in a survey of 100 serous ovarian carcinoma samples compared with 50 normal oviduct-matched tissues (13), miR-450a was among the most significantly altered miRNAs, presenting a 5-fold reduced expression.

While the previous studies suggest that miR-450a may function as a tumor suppressor in ovarian cancer, its function remains poorly understood. Here, we characterized miR-450a functions and identified some of its targets through *in vitro* and *in vivo* assays with ovarian cancer cell lines. We found that miR-450a expression results in suppression of genes involved in cell migration and extracellular matrix organization and dysregulation of epithelial-to-mesenchymal transition (EMT) pathway genes. miR-450a expression decreased cell clonogenicity, migration, and invasion *in vitro* and also decreased tumor growth in an *in vivo* xenographic model, suggesting tumor suppressive effects. Direct miR-450a targets were related to mitochondrial metabolism, including *TIMMDC1*, *MT-ND2*, *ACO2*, and *ATP5B*—genes that have also shown reduced expression in ovarian cancer. Consistently, miR-450a–overexpressing cells exhibited decreased glutaminolysis and increased glycolysis rates. This change in energetic metabolism may result in less efficient production of lipids, amino acids, nucleic acids, and NADPH, and then inhibition of signaling pathways associated with migration and invasion (14–16).

Materials and Methods

Cell culture maintenance

We used the commercial human cell lines A2780, purchased from the Cell Bank of Rio de Janeiro (BCRJ), and SKOV-3, kindly donated by the Molecular Oncology Research Center (MORC) at Barretos Cancer Hospital (Barretos, Brazil). A2780 and SKOV-3 were cultivated either in RPMI medium (Gibco, catalog no. 31800–022) or in DMEM (Gibco, catalog no. 11995065), respectively, supplemented with 10% FBS (GE Healthcare, catalog no. SH30071.03) and 100 units of penicillin and 0.1 mg/mL of streptomycin (Sigma-Aldrich Co., catalog no. P4333). Cells were cultivated at 37°C and 5% CO_2. The cell lines were checked for *Mycoplasma* once at 3 months using MycoAlert PLUS Mycoplasma Detection Kit (Lonza, catalog no. LT07-705) or Universal Mycoplasma Detection Kit (ATCC, catalog no. 30-1012K). A2780 and SKOV-3 cell lines were authenticated by BCRJ and MORC, respectively, using short tandem repeat DNA typing according to the International Reference Standard for Authentication of Human Cell Lines (17).

Plasmid construction and transduction

Expression vectors containing GFP and the pri-miR-450a or pri-miR-450b sequences were constructed with the pLVX-IRES-ZsGreen Vector as backbone (Clontech, catalog no. 632187, modified for restriction enzymes positions) using the *Eco*RI and *Bam*H1 restriction enzymes (New England Biolabs catalog nos. R0101S and R0136S, respectively) for cloning. DNA prepared from peripheral blood mononuclear cells was used as template to amplify the pri-miRNAs sequences with the following primers: miR-450a Forward: 5′-attgataGGATCCgaggctatcaggaagtat-3′, miR-450a Reverse: 5′-gctgagaGAATTCataattctgcatcttacat-3′, and miR-450b Forward: 5′-attgataGGATCCaagatggagggaataagc-3′, miR-450b Reverse: 5′-gctgagaGAATTCgagaaaaacaaacattacc-3′. The capital letters indicate the restriction site for *Bam*HI (GGATCC) and *Eco*RI (GAATTC) enzymes. The amplified DNA was introduced into the pLVX-IRES-ZsGreen using standard cloning procedures. Lentivirus was generated in 293FT cells (Thermo Fisher Scientific, catalog no. R70007) with ViraPower Packaging Mix (Thermo Fisher Scientific, catalog no. K4975-00) according to the manufacturer's protocol. Briefly, 3×10^6 293FT cells were plated and then cotransfected with Lipofectamine 2000 Transfection Reagent (Thermo Fisher Scientific, catalog no 11668027) after 24 hours with lentiviral package mix and pLVX-IRES-ZsGreen vectors. After 48 hours, 10^5 A2780 and SKOV-3 cells plated the day before were infected with total supernatant (purified with 0.45 μmol/L pore size filter) from 293FT cells for 2 times. GFP-positive cells were sorted by FACS to isolate cell lines stably expressing miR-450a and b.

Anoikis assay

We plated 10^5 cells in ultralow attachment 6-well plates (Corning Costar, catalog no. CLS3471-24EA). After 24 hours, recovered cells were trypsinized to obtain a single-cell suspension. We marked cells with FITC Annexin V Apoptosis Detection Kit I (BD Biosciences, catalog no. 556547) using Annexin V APC (BD Biosciences, catalog no. 550474) instead of Annexin V FITC, according to the manufacturer's instructions. At the moment of FACS analysis, we added to 200 μL of cells in PBS 1×, 50 μg/mL of propidium iodide (PI; BD Biosciences, catalog no. 5506463). Cells were analyzed on a FACS Caliber Flow Cytometer (BD Biosciences). Percentage of anoikis was calculated as cells Annexin V positive and PI negative. Cells negative for both markers were considered as viable.

Migration and invasion assays

Cell migration was evaluated in 24-well transwell inserts (Greiner Bio-One, catalog no 662638). Matrigel Invasion Chamber (Corning, catalog no. 354480) were used to perform the invasion assay. Before the assays, cells were serum-starved for 24 hours. In the top part of the chamber we added 5×10^5 or 2×10^4 cells for A2780 and SKOV-3 cell lines, respectively, in incomplete medium (without FBS) and complete medium to the bottom well. After 24 or 3 hours for A2780 and SKOV-3 cell lines, respectively, cells were removed from the top compartment with a cotton swab and cells that migrated to the lower face of the filter were fixed in 4% formaldehyde (in PBS) and stained with 0.5% crystal violet. For each insert, five fields of view including top, bottom, left, and right were photographed, and the average of cells was manually counted using Image J software.

Clonogenic assay

We synchronized the cells before the experiment by removing FBS from medium for 48 hours (5% in the first day and 0% in the second day). Single cells were plated in a 6-well plate and after 9 days they were fixed in 4% formaldehyde (in PBS), stained with 0.5% crystal violet and colonies formed by at least 50 cells were counted manually.

Xenograph model of ovarian cancer

All procedures were performed after approval of the National Council for the Control of Animal Experimentation and the Local Animal Ethical Committee from Ribeirão Preto Medical School of the University of São Paulo (Protocol no 141/2016). We used 9–11 weeks old NSG female mice and injected 5×10^6 cells of the control A2780 or A2780 cells expressing miR-450a and b into the peritoneal cavity. Animals were monitored during the time of experiment for tumor growth and after 4 weeks, 7–8 mice were sacrificed by anesthetic overdose using thiopental 150 mg/kg for 10 minutes and then lidocaine 2% in 5 mg/kg dose. The tumors from abdominal area were collected and weighed.

qRT-PCR

Reverse transcription was performed with High Capacity cDNA Reverse Transcription Kit (Thermo Fisher Scientific, catalog no. 4368813), according to the manufacturer's instructions. The qPCR for mRNA quantification of EMT markers from Fig. 1 (CDH1, VIM, TWIST1, and SERPINE1) was performed using TaqMan Universal PCR Master Mix (Thermo Fisher Scientific, catalog no. 4304437) and probes (Thermo Fisher Scientific, catalog nos. Hs01023894_m1, Hs0185584_m1, Hs00361186_m1, and Hs01126604_m1, respectively). Probes from rRNA 18s (Thermo Fisher Scientific, catalog no. Hs99999901_s1) and GAPDH (Thermo Fisher Scientific, catalog no. Hs02786624_g1) were used to normalize the expression. The other genes (ACO2, TIMMDC1, MT-ND2, ATP5B, and VIM from Fig. 4) had their expression measured using Power SYBR Green PCR Master Mix (Thermo Fisher Scientific, catalog no. 4367659). Their expression was normalized to TUBB and HPRT1, quantified with previously described primers. All reactions were done on a 7500 Fast Real-Time PCR System Cycler (Thermo Fisher Scientific). We calculated the relative expression using the $2^{-\Delta\Delta C_t}$ method (18) considering the samples with empty vector as the reference.

The sequences from designed primers are the following: ACO2 Forward: 5′-AGCCCAACGAGTACATCCAT-3′, ACO2 Reverse: 5′-TCTTCTCCGAGAGTGTCAGC-3′; ATP5B Forward: 5′-TGTTTGCTGGTGTTGGTGAG-3′, ATP5B Reverse: 5′-GAGCACCAGGTGGTTCATTC-3′; MT-ND2 Forward: 5′-CCCAACCCGTCATCTACTCT-3′, MT-ND2 Reverse: 5′-AAATCAGTGCGAGCTTAGCG-3′; TIMMDC1 Forward: 5′-CTACAGCAGGCATCATTGGC-3′, TIMMDC1 Reverse: 5′-TGCAGATTGCACAGCATCAA-3′; VIM Forward: 5′-CCCTGAACCTGAGGGAAACT-3′, VIM Reverse: 5′-ATTGCTGCACTGAGTGTGTG-3′, HPRT1 Forward: 5′-GAACGTCTTGCTCGAGATGTGA-3′, HPRT1 Reverse: 5′-TCCAGCAGGTCAGCAAAGAAT-3′; and TUBB Forward: 5′-TCAACACTTTCTTCAGTGAAACG-3′ TUBB Reverse: 5′-AGTGCCAGTGCGAACTTCATC-3′.

Western blot analysis

Whole-cell lysates were obtained by sonication of cells at 20% of amplitude for three cycles of 10 seconds in RIPA or IP (Tris 20 mmol/L, pH 7.5; NaCl 150 mmol/L; EDTA 2 mmol/L, and NP40 1%) buffers. Total protein amount in the lysate was determined using Bio-Rad Protein Assay Kit (Bio-Rad, catalog no. 5000001) and BSA as standard. Protein (20 μg) was loaded into the gel and transferred to nitrocellulose using standard blotting procedure. Protein expression was normalized to LAMIN A/C. For proteins difficult to detect in whole lysates (ATP5B and MT-ND2), we used the Mitochondria Isolation Kit for Cultured Cells (Thermo Fisher Scientific, catalog no. 89874) and VDAC3 antibody (Proteintech, catalog no. 14451-1-AP) (1:500 dilution) to normalize the expression. We used the following primary antibodies: AGO2 (Abcam, catalog no. ab32381) (1:2,000 dilution), HNRPA0 (1:2,000 dilution; Bethyl, catalog no. A303-941A) to normalize the whole-cell lysates expression, ACO2 (Proteintech, catalog no. 11134-1-AP; 1:500 dilution), VIM (Proteintech, catalog no. 10366-1-AP; 1:5,000 dilution), TIMMDC1 (Proteintech, catalog no. 23622-1-AP; 1:500 dilution), MT-ND2 (ABclonal, catalog no. A6180; 1:500 dilution), and ATP5B (Sigma, catalog no. HPA001528; 1:500 dilution). Membranes were developed with Luminata Crescendo Western HRP Substrate (Millipore, catalog no. WBLUR0500). Nuclear and cytoplasmic fractions from A2780 cell lines were obtained according to Adam and colleagues (19). In this assay we used Anti-pan Ago (1:500 dilution; Millipore-Sigma, catalog no. MABE56), HNRPA0, as previously mentioned, and GAPDH (1:2,000 dilution; Cell Signaling Technology, catalog no. 14C10) as primary antibodies. Bands were quantified using Image J software.

RNA-seq

Total RNA was extracted from three biological replicates from each cell line using TRizol Reagent (Invitrogen, catalog no. 15596026) according to the recommendations from the manufacturer. We used the NEBNext Ultra Directional RNA Library Prep Kit for Illumina (NEB, catalog no. E7760) with NEBNext rRNA Depletion Kit (NEB, catalog no. E6318). The samples were sequenced on an Illumina HiSeq 3000 machine using the 50 cycle single-read protocol. Sequence reads were aligned to the human genome h19 using TopHat. Differential gene expression was quantified using Cufflinks and Cuffdiff (20).

Small RNA-seq

For small RNA cDNA library, we followed the protocol from Farazi and colleagues (21) after RNA extraction. Samples were sequenced as described in previous item.

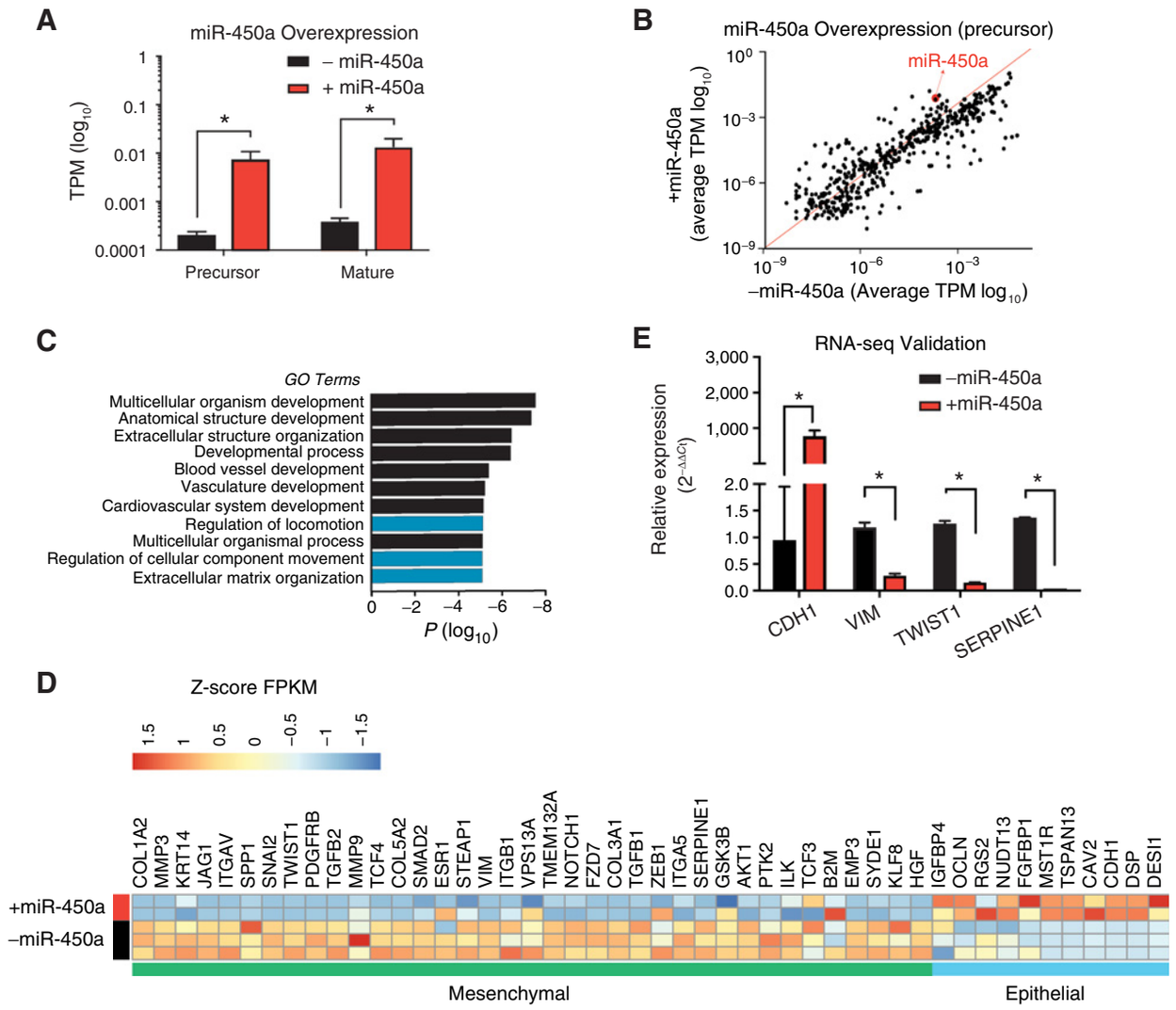

Figure 1.

miR-450a overexpression in A2780 cell line altered the expression of important EMT markers. **A** and **B,** Validation of miR-450a overexpression by small RNA-seq. **C,** GO enrichment analysis of top 100 genes downregulated after miR-450a overexpression in A2780 cell line. **D,** Heatmap with some EMT markers in control and miR-450a–overexpressed samples from RNA-seq. **E,** RNA-seq validation of some EMT markers with qPCR. – miR-450a, empty vector; + miR-450a, pri-miR-450a. The values refer to the average of three biological samples. *, $P < 0.05$.

AGO-PAR-CLIP

AGO 4SU-PAR-CLIP method was performed in two biological replicates as described previously (22, 23). Resulting cDNA libraries were sequenced on an Illumina HiSeq 3000 machine as single reads with 50 cycles. Analysis was performed as described previously using PARalyzer (24) built into the PARpipe (24) pipeline. Putative miR-450a targets were selected on the basis of the presence of the seed complementary sequence of miR-450a in binding sites not found in the AGO2 PAR-CLIP from the A2780 control sample.

Correlation analysis with The Cancer Genome Atlas data

To calculate correlation between the expression of the miRNA miR-450a-5p and PAR-CLIP targets using data from The Cancer Genome Atlas (TCGA) Research Network: http://cancergenome.nih.gov/, we downloaded the published RNA- and miRNA-Seq data for serous ovarian cystadenocarcinoma samples at https://tcga-data.nci.nih.gov/docs/publications/ov_2011/ by the cgdsr package (25) in R software (26). Expression levels were expressed in RSEM for mRNAs and TPM for miR-450a.

Mitochondrial membrane potential assay

A total of 2×10^5 cells of the A2780 and A2780 cell lines stably expressing miR-450a were grown in 24-well plates using standard conditions (see above). Before the experiment, cells were cultured for 30 minutes in DMEM (Thermo Fisher Scientific, catalog no. 21063029) without phenol red supplemented with 100 units of penicillin and 0.1 mg/mL of streptomycin and TMRM (Tetramethylrhodamine methyl ester, perchlorate;

Thermo Fisher Scientific, catalog no, I34361) at a final concentration of 20 nmol/L. Cells were collected by centrifugation at 1,200 rpm, washed with PBS, and centrifuged again. Cells were resuspended in the same medium and incubated in for 1 hour in FACS tubes at 37°C and 5% CO_2. Prior to fluorescence measurement of TMRM (laser: 488 nm, filter 585/42 BP) on a FACSCanto Machine (BD Biosciences) SORP, 1 μL of 0.01 mmol/L TO-PRO-3 Iodide (Thermo Fisher Scientific, catalog no. T3605; laser: 633 nm, filter 660/20 BP) was added to verify cell viability.

Glucose uptake assay

Glucose uptake assay was performed using the Glucose Uptake-Glo Assay (Promega, catalog no. J1341) according to the manufacturer's instructions.

Glutamate and glutamine assay

Glutamate and glutamine assay were performed using the Glutamine/Glutamate-Glo Assay (Promega, catalog no. J8021) according to the manufacturer's instructions.

Viability assay after glutamine removal

A total of 2×10^5 cells from A2780 cell lines were cultivated for 24 hours in DMEM (Thermo Fisher Scientific, catalog no. A14430) without glucose, glutamine, and phenol red, supplemented with 5% FBS, 100 units of penicillin and 0.1 mg/mL of streptomycin and 5 mmol/L D-glucose (Sigma, catalog no. G8644-100ML). Next, medium was removed and exchanged for DMEM with 5 mmol/L glucose and 100 units of penicillin and 0.1 mg/mL of streptomycin. Subsequently, cells were cultivated for more 24 hours and their viability was measured using Annexin V APC (BD Biosciences, catalog no. 550474) and PI (BD Biosciences, catalog no. 5506463) at FACS Caliber Flow Cytometer (BD Biosciences).

Statistical analysis

The expression and functional data were analyzed using Student *t* test or ANOVA, followed by Bonferroni posttest. To verify correlation regarding the expression of miRNAs and their targets in TCGA data, we used Spearman correlation coefficient. All the statistical analysis was performed with GraphPad Prism 7 software and $P < 0.05$ was considered as significant.

Data depository

RNA-seq, small RNA-seq, and PAR-CLIPs were deposited online in the Gene Expression Omnibus under accession number GSE129076.

Results

miR-450a decreased the expression of mesenchymal markers in ovarian cancer cells

To characterize the role of miR-450a in ovarian cancer, we manipulated the ovarian cancer cell line A2780 to stably express miR-450a using lentiviral transduction and confirmed overexpression of miR-450a by small RNA-seq (Fig. 1A and B; ref. 27). To quantify the impact of miR-450a overexpression on the transcriptome we used RNA-seq and compared A2780 cells with and without miR-450a expression. Analysis of the top 100 downregulated genes revealed that biological processes associated with miR-450a overexpression were categorized into gene ontology (GO) terms such as "regulation of locomotion," "regulation of cellular component movement," and "extracellular matrix organization" (Fig. 1C). Consistent with these enriched GO terms, the expression of many mesenchymal marker genes, including *VIM*, *TWIST1*, and *SERPINE1* decreased and some epithelial marker genes, for example, *CDH1*, increased in a panel of EMT genes (Fig. 1D). We validated some of these results using qPCR (Fig. 1E).

miR-450a has tumor suppressive effects *in vitro* and *in vivo*

As miR-450a overexpression resulted in widespread changes in genes associated with EMT, we tested whether it would affect cell migration and invasion. Indeed, overexpression of miR-450a reduced the migration and invasion rates of A2780 cells in transwell assays (Fig. 2A and B). Similar results were observed using another ovarian cancer cell line, SKOV-3 (Supplementary Fig. S1A and S1B), corroborating a general role for miR-450a in EMT regulation in ovarian cancer cells.

Because EMT is dependent on the ability of cells surviving in a deficient cell–matrix interaction context, we considered the possibility of miR-450a being involved in resistance to anoikis, a type of programmed cell death induced by lack of cell–matrix interactions (28). Overexpression of miR-450a decreased the viability of cells upon cultivation for 24 hours in nonadherent plates, reflecting an increase in the anoikis rate in A2780 (Fig. 2C) and SKOV-3 cells (Supplementary Fig. S1C). A successful EMT program in the cancer context depends on the capability of single cells to survive and produce new colonies in distant organs. Consistent with a function as tumor suppressor, miR-450a also decreased the colony-formation capacity of A2780 cells (Fig. 2D).

We next tested whether miR-450a would also have a tumor suppressor effect *in vivo*. NOD/SCID female mice injected intraperitoneally with A2780 cells stably overexpressing miR-450a presented fewer and significantly smaller tumors than animals injected with control cells (Fig. 2E), further strengthening our hypothesis that miR-450a has tumor suppressive effects.

miR-450b shows similar function as miR-450a

miRNAs guide the RISC to sites on target mRNAs based on complete or partial sequence complementarity and miRNAs from the same sequence family are expected to regulate a similar set of targets (Supplementary Fig. S2A; ref. 3) with similar effects *in vitro* and *in vivo*. We performed the same set of experiments described in Figs. 1 and 2 using cell lines stably overexpressing miR-450b (Supplementary Fig. S2B and S2C). Again, GO analysis of the 100 most downregulated genes in RNA-seq experiments from A2780 cells revealed that miR-450b affected similar processes as miR-450a, such as "regulation of cell motility," "locomotion," and "cellular component movement" (Supplementary Fig. S2D). miR-450b also inhibited the migration and invasion of the A2780 and SKOV-3 cell lines (Supplementary Fig. S2E and S2F). Finally, we confirmed that miR-450b reduced tumor growth in NOD/SCID female mice (Supplementary Fig. S2G and S2H). Taken together, our results indicate that both members of the miR-450 family had tumor suppressive function *in vitro* and *in vivo*, likely by targeting a similar set of transcripts.

Many targets of miR-450a-5p are associated with mitochondrial metabolism

To experimentally identify target genes of miR-450a, we mapped AGO protein interaction sites in A2780 cells and A2780 cells expressing miR-450a using 4-thiouridine (4SU) photoactivatable

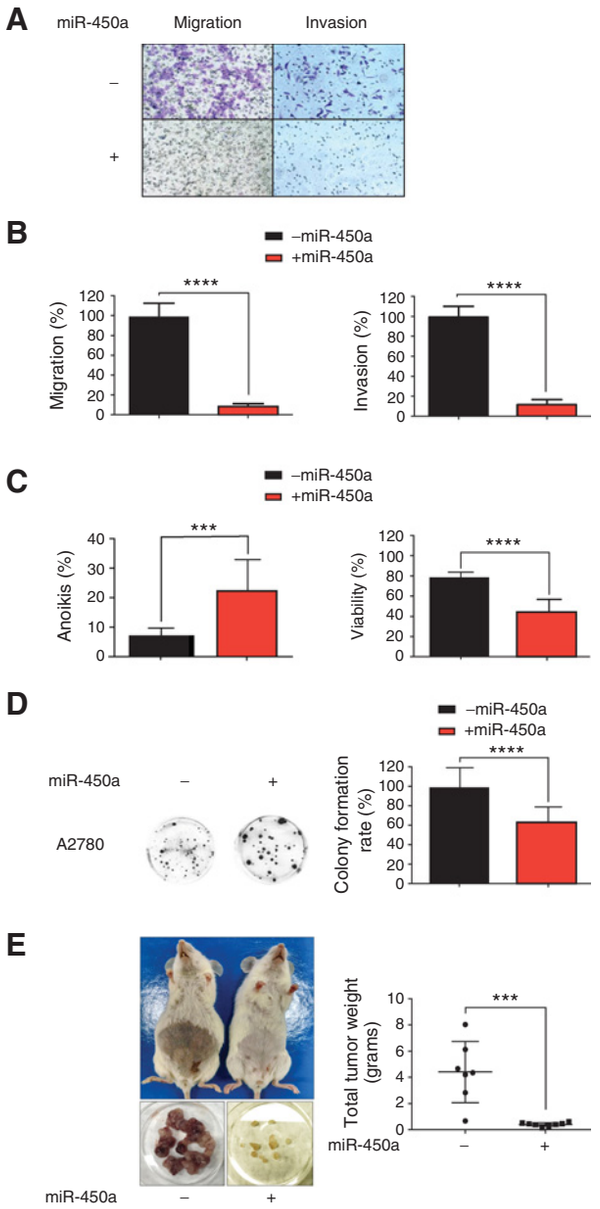

Figure 2.

miR-450a has tumor suppressor effects. **A,** Representative images from inserts after cell migration and invasion assays. **B,** Migration and invasion quantifications. **C,** Percentage of anoikis (percentage of Annexin V–positive cells, left) and viability (percentage of Annexin V- and PI-negative cells, right). **D,** Representative images from colonies after clonogenic assay (left) and colony formation rate (right). Each value was calculated, setting 100% as the number of cells that migrated or invaded in the control groups. –miR-450a, empty vector; +miR-450a, pri-miR-450a. The values refer to the average of three biological experiments. **E,** Representative images from tumors collected in each mouse (bottom) and mice before tumor collection (top; right). Tumor weights collected from all tumors in each mouse at the end of the experiment (left). The values refer to the average of 7–8 animals. ***, $P < 0.001$; ****, $P < 0.0001$.

ribonucleoside–enhanced cross-linking and immunoprecipitation (PAR-CLIP; ref. 22). We either isolated AGO2 with antibodies, or all expressed AGO proteins (AGO1–4) with a specific peptide derived from the AGO-interacting domain of the TNRC6 protein family (29).

Autoradiography of the cross-linked, ribonuclease-treated, and radiolabeled precipitate revealed one main band at approximately 100 kDa, corresponding to the expected size of the AGO-containing ribonucleoprotein (RNP) complex (Fig. 3A). We recovered the bound RNA fragments from the isolated AGO2 or AGO1–4-containing RNPs and generated small-RNA cDNA libraries for next-generation sequencing. We used the PARalyzer software (24) to determine clusters of overlapping reads

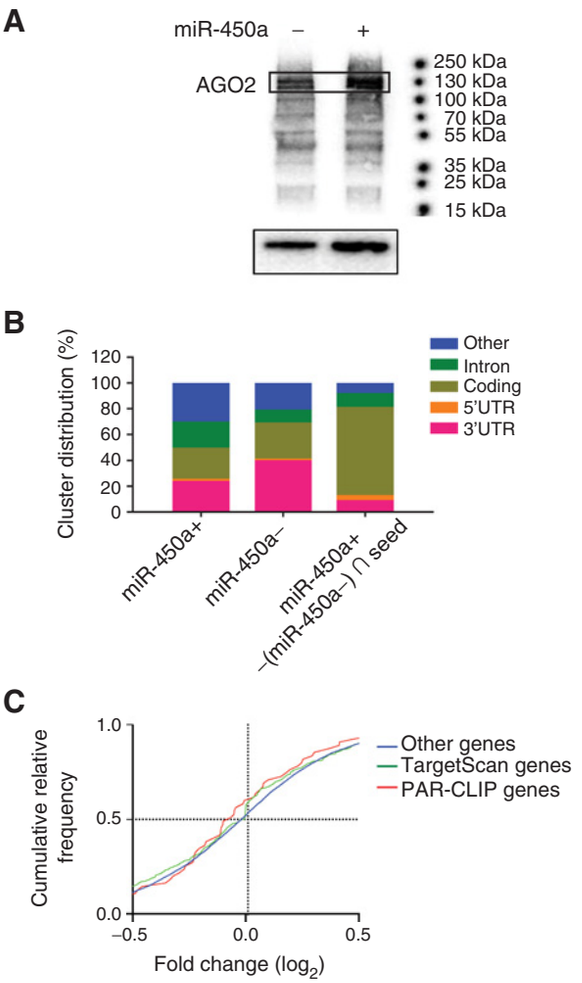

Figure 3.

PAR-CLIP analysis of A2780 cell lines. **A,** Recovery of AGO and RNAs bound to it after cross-link and autoradiography from SDS-PAGE of marked ATP [γ-32P] RNAs (top) and protein recovered from pulldown with TNRC6B peptide or antibody anti-AGO2 (bottom). The AGO2 protein corresponds to 130 kDa. – miR-450a, empty vector; + miR-450a, pri-miR-450a. **B,** Distribution of recovered RNA bound to AGO regarding their classification or mRNA-specific region. + miR-450a, pri-miR-450a; control, empty vector; (+450a - control) ∩ seed, RNAs exclusively found in miR-450a–overexpressed sample that contains the miR-450a complementary seed sequence. These distributions are relative to the results from best PAR-CLIPs replicate. **C,** Cumulative relative frequency of fold change (control samples vs. miR-450a–overexpressed samples) of genes recovered from RNA-seq analysis regarding their presence in PAR-CLIP experiments or TargetScan algorithm prediction.

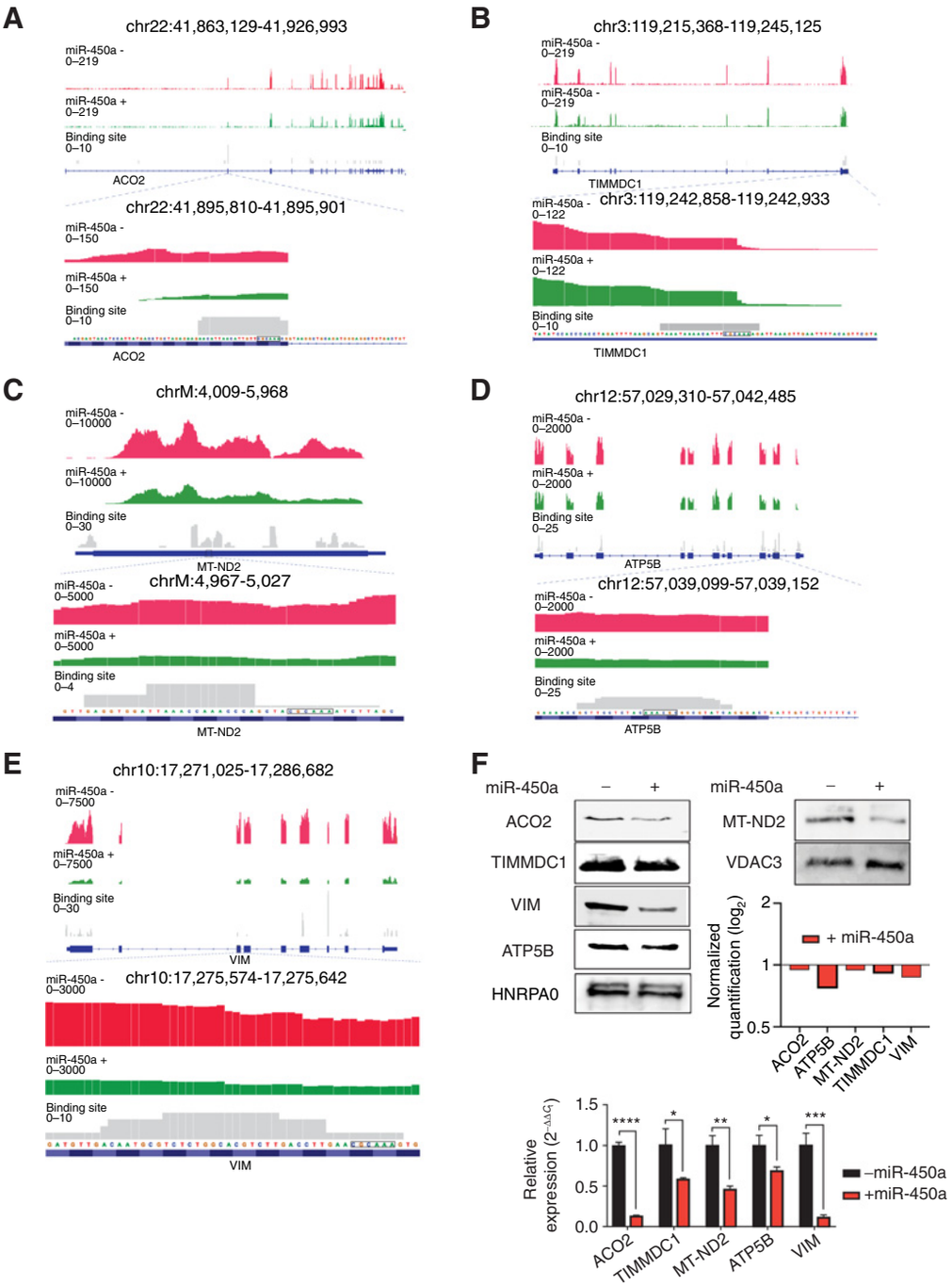

Figure 4.

miR-450a-5p directly targets ACO2 (**A**), TIMMDC1 (**B**), MT-ND2 (**C**), ATP5B (**D**), and VIM (**E**). Representative figure showing the frequency of reads derived from RNA-seq and PAR-CLIP (binding site track) in respective genes regions (top). **F**, Protein blots and their quantifications normalized against VDAC3 or HNRPA0 and empty vector samples (top) and qRT-PCR (bottom) from target genes. The qRT-PCR values refer to the average of three biological samples. VDAC3 or HNRPA0 was loaded as control in mitochondrial lysate and total lysate, respectively. –, empty vector; + miR-450a, pri-miR-450a. *, $P < 0.05$; **, $P < 0.01$; ***, $P < 0.001$; ****, $P < 0.0001$.

containing T-to-C mutations diagnostic of the cross-linking event. Considering that we were interested to comprehensively identify possible miR-450a–binding sites, we pooled the PAR-CLIP results generated from AGO2 immunoprecipitation or AGO1–4 pull-down from two best biological replicates in A2780 cells with and without miR-450a expression and found 11196 and 13497 potential miRNA binding sites, respectively. Of those, nine showed seed sequence complementarity to miR-450a in the

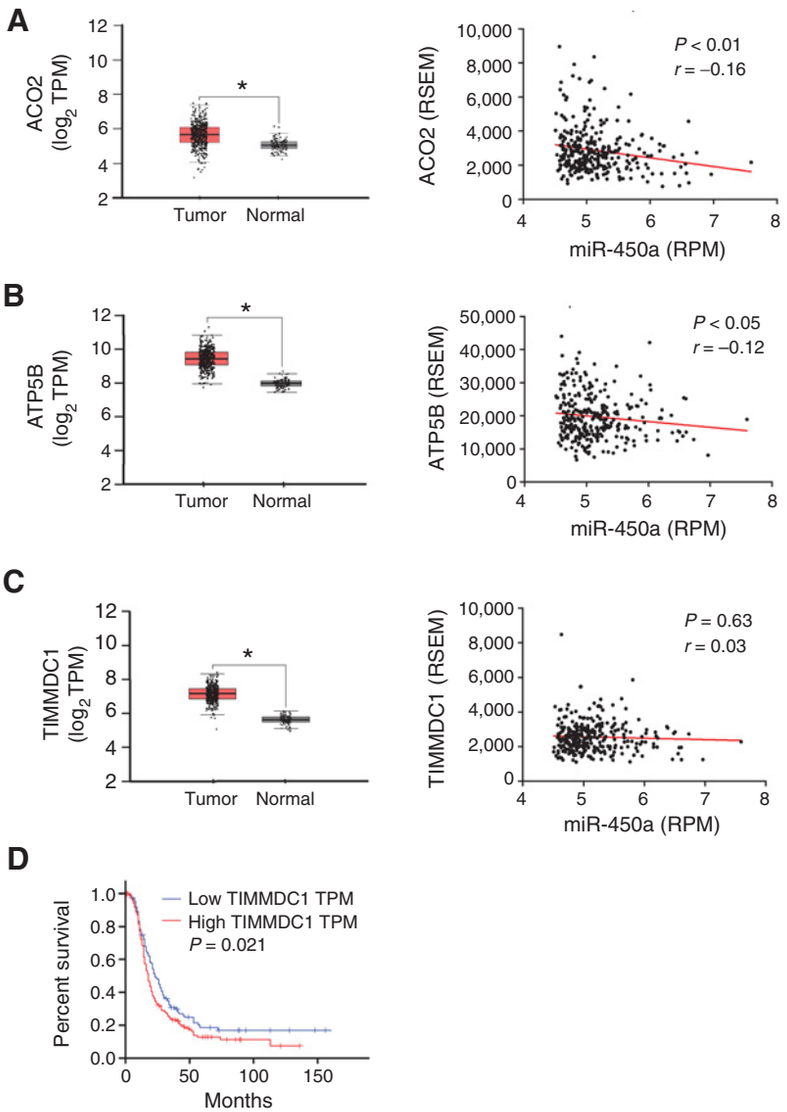

Figure 5.

ACO2 (**A**), ATP5B (**B**), and TIMMDC1 (**C**) are overexpressed in tumor ovarian tissues compared with normal ones. Left, boxplots showing the differential expression of the indicated genes between ovarian serous cystadenocarcinoma and Gtex normal samples. (Figures modified from gepia database: http://gepia.cancer-pku.cn/). Right, Spearman correlation between expression levels of miR-450a-5p and genes *ACO2, ATP5B*, and *TIMMDC1* in ovarian serous cystadenocarcinoma samples from TCGA data. Data were downloaded from cgdsr package in R software. $N = 294$ for tumor tissues. **D,** Disease-free survival from patients derived from TCGA ovarian serous cystadenocarcinoma samples database. (Figure modified from gepia database: http://gepia.cancer-pku.cn/). $N = 426$ for tumor tissue and $N = 88$ for normal tissue samples. *, $P < 0.05$.

control cell line compared with 53 in the miR-450a–expressing cell line (Supplementary Table S1A for control cell line and S1B for miR-450a–overexpressed cell line).

Most of the AGO-binding sites in these cell lines distributed to the mature mRNA and specifically the 3′ untranslated region, as expected of miRNA-binding sites in most cell lines (3, 30) and consistent with the mainly cytoplasmic localization of AGO proteins in A2780 (Supplementary Fig. S3). Nevertheless, most of the *bona fide* miR-450a–binding sites that contained (i) the miR-450a seed complementary sequence and (ii) were almost exclusively found in A2780-expressing miR-450a were found in mRNA-coding sequences (Fig. 3B).

We next confirmed that miR-450a indeed directly repressed its target genes in the RNA-seq datasets used above (Fig. 1). We binned mRNAs according to whether they did or did not contain a miR-450a target site either predicted by Targetscan (31) or by PAR-CLIP. Indeed, miR-450a expression tended to lead to a global decrease in abundance of predicted miR-450a target mRNAs compared with nontarget mRNAs (Fig. 3C), confirming that our approach was capturing functional miR-450a targets.

We noticed that many of the potential miR-450a targets we captured (pooled from four different experiments; Supplementary Table S2), were found in mRNAs encoding mitochondrial genes. We verified for a panel of those (ACO2, TIMMDC1, ATP5B, and MT-ND2) that miR-450a expression resulted in decreased mRNA abundance by RNA-seq and qRT-PCR, and concomitantly decreased protein abundance (Fig. 4A–F). Furthermore, VIM, the typical mesenchymal marker, is also among the possible miR-450a target genes downregulated upon miR-450a expression.

We further explored the expression of TIMMDC1, ATP5B, and ACO2 in ovarian cancers and their relationship with miR-450a. Using data from TCGA database, we compared expression levels of these genes in ovarian tumors with normal tissue and found that they were all significantly reduced in tumors. For ACO2 and ATP5B we further found a negative correlation of their expression levels with miR-450a, suggesting that these mRNAs are indeed

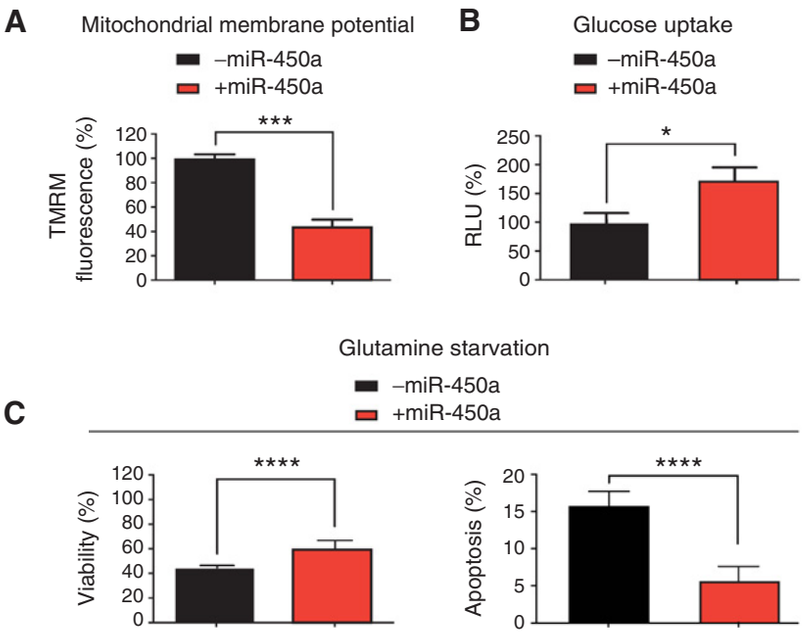

Figure 6.
Specific metabolic effects from miR-450a. **A,** miR-450a decreases mitochondrial membrane potential in A2780 cell line. **B,** miR-450a increases glucose uptake in A2780 cell line. **C,** miR-450a increases viability (left) and decreases apoptosis (right) under glutamine removal in A2780 cell line. The values refer to the average of three different experiments. −, empty vector; + miR-450a, pri-miR-450a. *, $P < 0.05$; ***, $P < 0.001$; ****, $P < 0.0001$.

direct targets of miR-450a *in vivo* (Fig. 5A–C). Of the examined genes, low TIMMDC1 expression levels were also clearly associated with disease-free survival (Fig. 5D).

miR-450a expression decreases mitochondrial membrane potential and increases glucose uptake and viability after glutamine withdrawal

Many of the directly bound and moderately downregulated miR-450a targets were associated with the mitochondrial oxidative phosphorylation complexes (complex I: TIMMDC1 and MT-ND2; complex V: ATP5B) and thus, we hypothesized that the rate of oxidative phosphorylation would be decreased in miR-450a–expressing cells. The oxidative phosphorylation rate is coupled to the mitochondrial membrane potential, which can be measured colorimetrically by staining with TMRM (32). Consistent with our hypothesis, overexpression of miR-450a in A2780 cell line resulted in more than 50% decrease in mitochondrial membrane potential compared with controls (Fig. 6A).

We next asked whether this decrease in membrane potential would result in a metabolic switch of miR-450a–expressing cells from oxidative phosphorylation to glycolysis. We used the 2-deoxyglucose-6-phosphate assay to quantify the cellular glucose uptake rate as an indicator of glycolysis and found it was increased by almost 80% upon miR-450a overexpression (Fig. 6B).

Next to glucose, glutamine is one of the main sources of energy for mammalian cells (33). A prominent miR-450a target was ACO2, which is part of the citric acid cycle and metabolizes α-ketoglutarate, a product of glutamine oxidation (34). We therefore asked whether miR-450a expression could alter cellular glutamine metabolism. We observed that miR-450a increased the viability of cells after glutamine withdrawal, likely by reducing apoptosis rates (Fig. 6C). In addition, miR-450a slightly decreased glutamate production, whereas glutamine uptake from the medium was moderately increased (Supplementary Fig. S4A and S4B). Our data suggest that miR-450a acts as a tumor suppressor by rewiring and acting as a break on cellular metabolism. Its overexpression increased the uptake of glucose; however, the cells exhibited impaired glutaminolysis and only efficiently used glycolysis for energy production.

Discussion

Reprogramming of energy metabolism is one of the hallmarks of cancer (35). Tumor cells actively divide and require more glucose to generate energy even under normal oxygen conditions. Typically, in most tumors, the pyruvate produced during glycolysis is converted into lactic acid rather than completely metabolized into carbon dioxide by oxidative phosphorylation (Warburg effect; ref. 36). Nevertheless, many types of cancers, including most ovarian tumors maintain a high rate of oxidative phosphorylation (36). In addition to requiring increased amounts of glucose, tumor cells may also become "glutamine addicted". These cells depend on glutaminolysis as a source of energy, but also for the production of lipids, amino acids, and nucleotides for cell replication (14, 15, 37), and of metabolites for the maintenance of mitochondrial membrane potential (14). Here we presented evidence that miR-450a act as a tumor suppressive molecule, most likely by directly targeting and suppressing key mitochondrial genes and rewiring the cellular metabolism to reduce glutaminolysis and oxidative phosphorylation (Fig. 7).

For example, we found and validated that miR-450a directly targets and suppresses ACO2 in ovarian cancer cells. ACO2 converts citrate into isocitrate and is a key enzyme in the citrate cycle, and involved in glutaminolysis (37). This is consistent with a previous report that found that highly invasive ovarian cancers, that avoid miR-450a expression, have higher rates of glutaminolysis than less invasive cells (16) and are more dependent on glucose and, therefore, on the glycolysis process. At the same time,

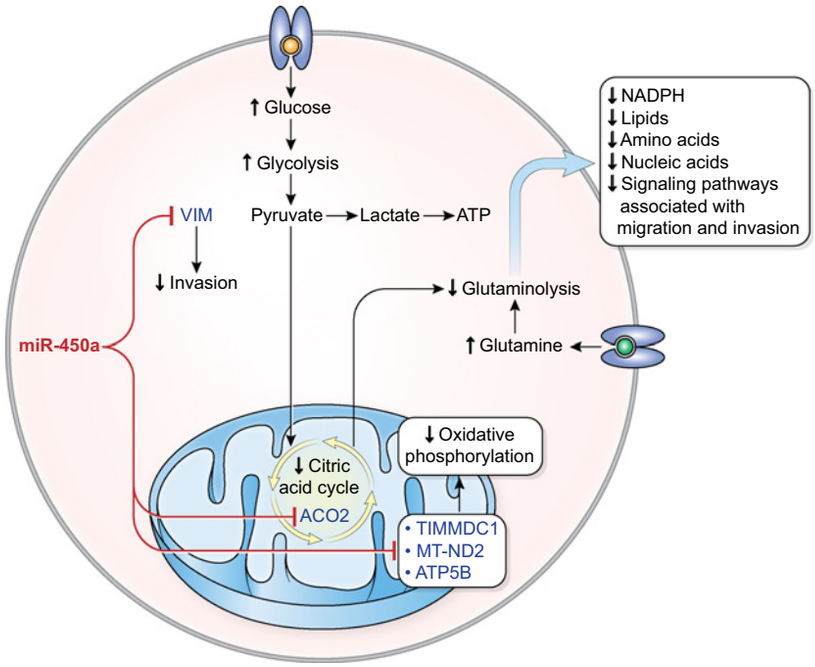

Figure 7.
Model proposed for action of miR-450a in ovarian cancer. miR-450a inhibits mitochondrial genes from complex I (TIMMDC1 and ND2) and complex V (ATP5B), which cause decreased oxidative phosphorylation rate. This leads to the increased consumption of glucose. As miR-450a also inhibits ACO2, an enzyme from citric acid cycle, most part of the glucose is probably metabolized directly in pyruvate (increased glycolysis rate, also known as Warburg effect). Moreover, because the citric acid cycle is important for glutamine metabolization, there is a decrease in glutaminolysis rate, which contributes to the decreased production of NADPH, lipids, amino acids, nucleic acids, and signaling pathways associated with migration and invasion. In addition, miR-450a can inhibit invasion through inhibition of VIM.

high expression of genes associated with the citric acid cycle, such as ACO2, was found correlated with shorter patient survival (16).

We also found that miR-450a impaired mitochondrial activity by downregulation of TIMMDC1 and MT-ND2 (genes from complex I in oxidative phosphorylation) and ATP5B (subunit of mitochondrial ATP synthase). This in turn increased the glucose uptake, which is a sign of higher rate of glycolysis. TIMMDC1 has oncogenic effects in lung (38) and gastric cancer cell lines (39) and consistent with our results, TIMMDC1 knockdown decreased the membrane potential in lung carcinoma cells (38). We suggest that the combined reduction of oxidative phosphorylation and glutaminolysis made our miR-450a–expressing cells on one hand less dependent on glutamine for survival, but also less aggressive compared with control cell line. In this way, miR-450a inhibits mitochondrial and citric acid cycle genes (*TIMMDC*, *ND2*, and *ACO2*, respectively) decreasing the oxidative phosphorylation levels, which in turn leads to an increase of glucose consumption and a decrease in glutaminolysis degree. This metabolic rewiring is the probable responsible for the decreased tumorigenic and metastatic potential of the cell, as the glutaminolysis rate is important for the generation of metabolites important for cell maintenance and metastasis. In addition, the inhibition of VIM contributes for this pattern.

Although is known that Wnt pathway can promote glutaminolysis (40), we did not find a direct association with this pathway from our RNA-seq data. Nevertheless, miR-450a has been demonstrated to target and downregulate WISP2, a Wnt-associated protein, in the context of adipogenesis (41). From our data, curiously, many genes associated to this pathway were upregulated after miR-450a overexpression like MYC and CTNNB1, what could be explained as a way of the cells trying to adapt to the metabolic shift caused by miR-450a.

To our knowledge, this is the first work demonstrating a miRNA-targeting nuclear (ACO2, ATP5B, and TIMMDC1) or mitochondrially (MT-ND2) encoded mitochondrial genes in the context of ovarian cancer. Although there is evidence that a number of miRNAs can target mitochondrially localized genes there is no well stablished mechanism of transport of miRNAs encoded in nucleus to mitochondria (42).

Taken together, we propose that miR-450a acts as a tumor suppressor that decreases the tumorigenicity and metastasis ability in ovarian cancer. The tumorigenicity is the ability to grow tumor from cells derived from culture after their injection in immunodeficient mice (43). The metastatic potential is the ability of tumor cells to migrate and invade other tissues and to survive in the absence of adhesion to the extracellular matrix during their pathway from one organ to another through the systemic circulation (44) or peritoneal fluid; a process that can be partially mimicked by cell dishes, which prevent cell adhesion (45). A reduction of tumorigenic and metastatic potential of miR-450a–expressing cells was corroborated by our *in vitro* and *in vivo* assays, that showed reduction of EMT markers expression and most prominently, of the canonical mesenchymal gene, *VIM*, a miR-450a target we validated. This effect was reinforced by the inhibition of oncogenes related to energetic metabolism (ACO2, ATPB5, MT-ND2, and TIMMDC1; refs. 38, 46–49).

Disclosure of Potential Conflicts of Interest

No potential conflicts of interest were disclosed.

Authors' Contributions

Conception and design: B.R. Muys, M. Hafner, W.A. Silva
Development of methodology: B.R. Muys, A.A. Sarshad, X. Wang
Acquisition of data (provided animals, acquired and managed patients, provided facilities, etc.): B.R. Muys, J.F. Sousa
Analysis and interpretation of data (e.g., statistical analysis, biostatistics, computational analysis): B.R. Muys, J.F. Sousa, J.R. Plaça, L.F. de Araújo, D.G. Anastasakis, G.A. de Molfetta, A. Lal, D.O. Vidal, W.A. Silva
Writing, review, and/or revision of the manuscript: B.R. Muys, J.F. Sousa, J.R. Plaça, G.A. de Molfetta, A. Ramão, D.O. Vidal, M. Hafner

Administrative, technical, or material support (i.e., reporting or organizing data, constructing databases): B.R. Muys, D.G. Anastasakis, X.L. Li, G.A. de Molfetta, W.A. Silva
Study supervision: B.R. Muys, G.A. de Molfetta, A. Lal, M. Hafner, W.A. Silva
Other (performed experiments): A.A. Sarshad

Acknowledgments

This work was financed by The National Council for Scientific and Technological Development (CNPq), grant #465539/2014-9; São Paulo Research Foundation (FAPESP), grants #2009/53853-5, #2013/08135-2, 2013/25119-0, #2013/25326-6, and #2016/22307-9, by the Intramural Research Program of the National Institute for Arthritis and Musculoskeletal and Skin Disease and NCI. We thank NIAMS Genomics Core Facility and Gustavo Gutierrez-Cruz and Dr. Stefania Dell'Orso (NIAMS/NIH) for sequencing support. We also thank Adriana Aparecida Marques, Anemari Ramos Dinarte dos Santos, Kamila Peroni, and Cleide Lúcia Araújo for the technical support.

The costs of publication of this article were defrayed in part by the payment of page charges. This article must therefore be hereby marked *advertisement* in accordance with 18 U.S.C. Section 1734 solely to indicate this fact.

Received February 19, 2019; revised April 12, 2019; accepted May 13, 2019; published first May 17, 2019.

References

1. Yokoi A, Matsuzaki J, Yamamoto Y, Yoneoka Y, Takahashi K, Shimizu H, et al. Integrated extracellular microRNA profiling for ovarian cancer screening. Nat Commun 2018;9:4319.
2. Lengyel E. Ovarian cancer development and metastasis. Am J Pathol 2010; 177:1053–64.
3. Bartel DP. Metazoan microRNAs. Cell 2018;173:20–51.
4. Lewis BP, Shih I, Jones-Rhoades MW, Bartel DP, Burge CB. Prediction of mammalian microRNA targets. Cell 2003;115:787–98.
5. Lai EC. Micro RNAs are complementary to 3′ UTR sequence motifs that mediate negative post-transcriptional regulation. Nat Genet 2002; 30:363–4.
6. Braun JE, Huntzinger E, Fauser M, Izaurralde E. GW182 proteins directly recruit cytoplasmic deadenylase complexes to miRNA targets. Mol Cell 2011;44:120–33.
7. Chekulaeva M, Mathys H, Zipprich JT, Attig J, Colic M, Parker R, et al. miRNA repression involves GW182-mediated recruitment of CCR4-NOT through conserved W-containing motifs. Nat Struct Mol Biol 2011;18: 1218–26.
8. Fabian MR, Cieplak MK, Frank F, Morita M, Green J, Srikumar T, et al. miRNA-mediated deadenylation is orchestrated by GW182 through two conserved motifs that interact with CCR4-NOT. Nat Struct Mol Biol 2011; 18:1211–7.
9. Friedman RC, Farh KK-H, Burge CB, Bartel DP. Most mammalian mRNAs are conserved targets of microRNAs. Genome Res 2008;19:92–105.
10. Croce CM. Causes and consequences of microRNA dysregulation in cancer. Nat Rev Genet 2009;10:704–14.
11. Dahiya N, Morin PJ. MicroRNAs in ovarian carcinomas. Endocr Relat Cancer 2010;17:F77–89.
12. Zhang L, Volinia S, Bonome T, Calin GA, Greshock J, Yang N, et al. Genomic and epigenetic alterations deregulate microRNA expression in human epithelial ovarian cancer. Proc Natl Acad Sci 2008;105:7004–9.
13. Li Y, Yao L, Liu F, Hong J, Chen L, Zhang B, et al. Characterization of microRNA expression in serous ovarian carcinoma. Int J Mol Med 2014;34: 491–8.
14. Wise DR, Thompson CB. Glutamine addiction: a new therapeutic target in cancer. Trends Biochem Sci 2010;35:427–33.
15. Daye D, Wellen KE. Metabolic reprogramming in cancer: Unraveling the role of glutamine in tumorigenesis. Semin Cell Dev Biol 2012;23: 362–9.
16. Yang L, Moss T, Mangala LS, Marini J, Zhao H, Wahlig S, et al. Metabolic shifts toward glutamine regulate tumor growth, invasion and bioenergetics in ovarian cancer. Mol Syst Biol 2014;10:728.
17. Dirks WG, Faehnrich S, Estella IAJ, Drexler HG. Short tandem repeat DNA typing provides an international reference standard for authentication of human cell lines. ALTEX 2005;22:103–9.
18. Livak KJ, Schmittgen TD. Analysis of relative gene expression data using real-time quantitative PCR and the 2(−delta delta C(T)) method. Methods 2001;25:402–8.
19. Adam SA, Marr RS, Gerace L. Nuclear protein import in permeabilized mammalian cells requires soluble cytoplasmic factors. J Cell Biol 1990; 111:807–16.
20. Trapnell C, Roberts A, Goff L, Pertea G, Kim D, Kelley DR, et al. Differential gene and transcript expression analysis of RNA-seq experiments with TopHat and Cufflinks. Nat Protoc 2012;7:562–78.
21. Farazi TA, Brown M, Morozov P, Ten Hoeve JJ, Ben-Dov IZ, Hovestadt V, et al. Bioinformatic analysis of barcoded cDNA libraries for small RNA profiling by next-generation sequencing. Methods 2012;58: 171–87.
22. Hafner M, Landthaler M, Burger L, Khorshid M, Hausser J, Berninger P, et al. Transcriptome-wide identification of RNA-binding protein and microRNA target sites by PAR-CLIP. Cell 2010;141:129–41.
23. Benhalevy D, McFarland HL, Sarshad AA, Hafner M. PAR-CLIP and streamlined small RNA cDNA library preparation protocol for the identification of RNA binding protein target sites. Methods 2017;118–9:41–9.
24. Corcoran DL, Georgiev S, Mukherjee N, Gottwein E, Skalsky RL, Keene JD, et al. PARalyzer: definition of RNA binding sites from PAR-CLIP short-read sequence data. Genome Biol 2011;12:R79.
25. Jacobsen A. cgdsr: R-based API for accessing the MSKCC Cancer Genomics Data Server (CGDS) version 1.2.6 from CRAN. https://rdrr.io/cran/cgdsr/.
26. R Development Core Team. R: A language and environment for statistical computing. Vienna, Austria: R Foundation for Statistical Computing; 2008. http://www.R-project.org/.
27. Hafner M, Renwick N, Farazi TA, Mihailović A, Pena JT, Tuschl T. Barcoded cDNA library preparation for small RNA profiling by next-generation sequencing. Methods 2012;58:164–70.
28. Frisch SM, Ruoslahti E. Integrins and anoikis. Curr Opin Cell Biol 1997;9: 701–6.
29. Hauptmann J, Schraivogel D, Bruckmann A, Manickavel S, Jakob L, Eichner N, et al. Biochemical isolation of Argonaute protein complexes by Ago-APP. Proc Natl Acad Sci U S A 2015;112:11841–5.
30. Sarshad AA, Juan AH, Muler AIC, Anastasakis DG, Wang X, Genzor P, et al. Argonaute-miRNA complexes silence target mRNAs in the nucleus of mammalian stem cells. Mol Cell 2018;71:1040–50.
31. Agarwal V, Bell GW, Nam J-W, Bartel DP. Predicting effective microRNA target sites in mammalian mRNAs. Elife 2015;4:e05005.
32. Perry SW, Norman JP, Barbieri J, Brown EB, Gelbard HA. Mitochondrial membrane potential probes and the proton gradient: a practical usage guide. Biotechniques 2011;50:98–115.
33. Mayers JR, Vander Heiden MG. Famine versus feast: understanding the metabolism of tumors *in vivo*. Trends Biochem Sci 2015;40:130–40.
34. DeBerardinis RJ, Chandel NS. Fundamentals of cancer metabolism. Sci Adv 2016;2:e1600200.
35. Hanahan D, Weinberg RA. Hallmarks of cancer: the next generation. Cell 2011;144:646–74.
36. Wallace DC. Mitochondria and cancer. Nat Rev Cancer 2012;12: 685–98.
37. Li C, Zhang G, Zhao L, Ma Z, Chen H. Metabolic reprogramming in cancer cells: glycolysis, glutaminolysis, and Bcl-2 proteins as novel therapeutic targets for cancer. World J Surg Oncol 2016;14:15.
38. Wu H, Wang W, Xu H. Depletion of C3orf1/TIMMDC1 inhibits migration and proliferation in 95D lung carcinoma cells. Int J Mol Sci 2014;15: 20555–71.
39. Liu Y, Huang Y, Zhang J, Pei C, Hu J, Lyu J, et al. TIMMDC1 knockdown inhibits growth and metastasis of gastric cancer cells through metabolic inhibition and AKT/GSK3β/β-catenin signaling pathway. Int J Biol Sci 2018;14:1256–67.
40. Sethi JK, Vidal-Puig A. Wnt signalling and the control of cellular metabolism. Biochem J 2010;427:1–17.

41. Zhang Y, Yu M, Dai M, Chen C, Tang Q, Jing W, et al. miR-450a-5p within rat adipose tissue exosome-like vesicles promotes adipogenic differentiation by targeting WISP2. J Cell Sci 2017;130:1158–68.
42. Vendramin R, Marine J-C, Leucci E. Non-coding RNAs: the dark side of nuclear-mitochondrial communication. EMBO J 2017;36:1123–33.
43. World Health Organization. Proposed requirements for continuous cell lines used for the preparation of biological products, with special reference to inactivated vaccines. Geneva, Switzerland: 1985. Available from: https://apps.who.int/iris/handle/10665/60734.
44. Kenific CM, Thorburn A, Debnath J. Autophagy and metastasis: another double-edged sword. Curr Opin Cell Biol 2010;22:241–5.
45. Kunjithapatham R, Karthikeyan S, Geschwind J-F, Kieserman E, Lin MD, Fu D-X, et al. Reversal of anchorage-independent multicellular spheroid into a monolayer mimics a metastatic model. Sci Rep 2014;4:6816.
46. Tsui K-H, Feng T-H, Lin Y-F, Chang P-L, Juang H-H. p53 downregulates the gene expression of mitochondrial aconitase in human prostate carcinoma cells. Prostate 2011;71:62–70.
47. Gusdon AM, Votyakova TV, Mathews CE. mt-Nd2a suppresses reactive oxygen species production by mitochondrial complexes I and III. J Biol Chem 2008;283:10690–7.
48. Li W, Li Y, Li G, Zhou Z, Chang X, Xia Y, et al. Ectopic expression of the ATP synthase β subunit on the membrane of PC-3M cells supports its potential role in prostate cancer metastasis. Int J Oncol 2017;50:1312–20.
49. Hjerpe E, Egyhazi Brage S, Carlson J, Frostvik Stolt M, Schedvins K, Johansson H, et al. Metabolic markers GAPDH, PKM2, ATP5B and BEC-index in advanced serous ovarian cancer. BMC Clin Pathol 2013;13:30.